

Clinical Imaging Findings of Oropharyngeal Tularemia: The Diagnostic Value of Imaging Findings

Orofaringeal Tulareminin Tıbbi Görüntüleme Bulguları: Görüntüleme Bulgularının Tanısal Değeri

Ömer KOÇAK¹, Aslı AYAN², A.Turan ILICA³, Banu ÇAKIR⁴, Yavuz ÇEKİLİ⁵,
Dilek KÖSEHAN⁶, Serdar KARAHATAY⁷, Muhammet UZUN⁸

¹Yüksek İhtisas University Medical Faculty, Department of Radiology, Ankara

²Gülhane Research and Training Hospital, Department of Nuclear Medicine, Ankara

³Memorial Sloan Kettering Cancer Center, Division of Neuroradiology, Department of Radiology, New York-US

⁴Ankara Atatürk Training and Research Hospital, Department of Radiology, Ankara

⁵Gülhane Research and Training Hospital, Department of Infectious Disease and Clinical Microbiology, Ankara

⁶Memorial Hospital, Department of Radiology, Ankara

⁷LIV Hospital, Department of Otolaryngology, Ankara

⁸Ankara Training and Research Hospital, MRI Department (Outsource service of ATL Health Corp.), Ankara

Abstract

Infection caused by *Francisella tularensis* may manifest as oropharyngeal tularemia (OT). The aim of this study was to characterize the imaging findings of this infection in the head and neck. The medical records and imaging examinations of 13 patients with serologically diagnosed OT were reviewed (8 US, 5 CT, 10 MRI, and 1 PET/CT). The typical presentation of OT (n=13) was an enlarged, non-tender neck mass that was unresponsive to conventional antibiotics. Clinical imaging tools revealed bilateral asymmetric lymphadenopathy with three different shapes: ellipsoid (n=2), round (n=9) and indistinct (n=2). Cutaneous extension and inflammatory stranding of the subcutaneous fat were observed in one patient. The lymph nodes involved level I (n=3), level II (n=11), level III (n=6), level IV (n=3), the parotid space (n=1), and the retropharyngeal space (n=2). US revealed lymph nodes with ellipsoid (n=2) or oval-round (n=6) shape. Three patients exhibited large, necrotic lymph nodes; one of the lymph nodes had invaded the surrounding tissue and could not be differentiated from the sternocleidomastoid muscle on sonography. In one patient, sonography revealed strong echoes within the lymph nodes due to calcifications. Loss of the normal nodal shape with spread into the subcutaneous tissue was observed in two patients. The lymph nodes showed central necrosis and ring enhancement (n=9) mostly in CT and MRI scans, exhibited diffusion restriction and displayed low ADC (apparent diffusion coefficient) values ranging from 0.691x10⁻³ mm²/s to 0.796x10⁻³ mm²/s. The one patient who underwent PET/CT, exhibited high FDG uptake (SUV=6.1) in the involved lymph nodes. In OT of the head and neck, most of the imaging features are not characteristic. However, some suggestive imaging features including low-density ring-enhancing LAP showing rare cutaneous extension, conglomeration and calcification including in the upper neck levels and the retropharyngeal space may be observed. Our data suggest that imaging could serve as an easy non-invasive method for the detection and classification of this disease for treatment planning.

Keywords: Imaging, Lymph Nodes, Oropharyngeal, Tularemia

Öz

Francisella tularensis kaynaklı enfeksiyonlar orofaringeal tularemi (OT) şeklinde kendini gösterebilir. Bu çalışmanın amacı baş ve boyunda görülen bu enfeksiyonun görüntüleme bulgularını tanımlamaktır. Serolojik olarak OT tanısı almış 13 hastanın tıbbi kayıtları ve görüntüleme tetkikleri gözden geçirildi (8 USG, 5 BT, 10 MRG ve 1 PET/BT). OT'nin (n=13) tipik prezentasyonu konvansiyonel antibiyotik tedavisine cevap vermeyen ağrısız, büyümüş boyun kitlesiydi. Görüntüleme tetkiklerinde elipsoid (n=2), yuvarlak (n=9) ve şekilsiz (n=2) olmak üzere üç farklı şekilde bilateral asimetrik lenfadenopatiler ile karşılaşıldı. Bir vakada cilde uzanım ve ciltaltı yağ dokusunda inflamatuvar çizgilenme görüldü. Lenf nodları seviye I (n=3), seviye II (n=11), seviye III (n=6), seviye IV (n=3), parotid mesafe (n=1) ve retrofaringeal mesafe (n=2) yerleşimliydi. USG'de izlenen lenf nodları elipsoid (n=2) veya oval-yuvarlak (n=6) şekilliydi. Üç hastada büyük ve nekrotik lenf nodları izlenmiş olup bu lenf nodlarının biri çevre dokuyu infiltre etmişti ve USG'de sternokleidomastoid kasından ayırt edilemiyordu. Bir hastada USG'de lenf nodları içerisinde kalsifikasyona bağlı belirgin ekojenite artışları kaydedildi. İki hastada normal nodal şekilde bozulma ve ciltaltı yumuşak dokuya yayılım mevcuttu. Lenf nodları BT ve MRG'de santral nekroz ve halkasal kontrastlanma (n=9), ayrıca difüzyon kısıtlanması ve 0.691 mm²x10⁻³ ile 0.796 mm²x10⁻³ arasında olacak şekilde düşük ADC değerleri gösterdi. PET/BT ile görüntülenen bir hastada enfekte lenf nodlarında yüksek FDG tutulumu (SUV=6.1) izlendi. Baş ve boyunda OT'inde bulgular çoğunlukla karakteristik değildir. Ancak, üst boyun seviyeleri ve retrofaringeal mesafede halkasal kontrastlanan düşük dansiteli lenfadenopatilerde nadir görülen cilt uzanımı, konglomerasyon ve kalsifikasyon gibi bulguların olması OT'yi düşündürülebilir. Çalışmamız bu hastalığın saptanması ve tedavi için sınıflandırılmasında tıbbi görüntülemenin kolay bir non-invaziv yöntem olduğuna işaret etmektedir.

Anahtar Kelimeler: Görüntüleme, Lenf Nodları, Orofaringeal, Tularemi

	ORCID No
Ömer KOÇAK	0000-0002-0143-2206
Aslı AYAN	0000-0001-6311-1785
A.Turan ILICA	0000-0002-8701-6042
Banu ÇAKIR	0000-0002-8508-528X
Yavuz ÇEKİLİ	0000-0002-0925-925X
Dilek KÖSEHAN	0000-0002-8889-7689
Serdar KARAHATAY	0000-0002-8391-4267
Muhammet UZUN	0000-0001-8669-7686

Başvuru Tarihi / Received: 29.07.2018

Kabul Tarihi / Accepted : 05.09.2018

Adres / Correspondence : Ömer KOÇAK
Yüksek İhtisas University Medical Faculty, Department of
Radiology, Ankara
e-posta / e-mail : omerkocak@me.com

Introduction

Tularemia, also known as rabbit fever, is a zoonotic disease caused by the virulent *Francisella tularensis* species and is characterized by a variety of clinical manifestations. It is most common in the northern hemisphere and can be caused by direct contact with infected rodents (e.g., squirrels, voles, rabbits, and muskrats), aerogenic exposure, ingestion of contaminated food or water, or by arthropod bites (e.g., ticks, mosquitos, and deer flies acting as vectors for the disease) (1, 2).

Oropharyngeal tularemia (OT) represents up to 12% of the overall cases (3). OT patients generally exhibit exudative pharyngitis or tonsillitis along with cervical lymphadenopathy (LAP) or abscess formation(1). Although the clinical, laboratory and therapeutic features of this entity are well known, its detailed imaging findings have not yet been described. Only one prior manuscript has focused on the CT findings of OT (4). The present manuscript describes the first advanced imaging characteristics of OT through the use of high resolution US, CT, MRI and PET/CT. Our goal is to highlight OT within the differential diagnosis of patients with oropharyngeal symptoms and LAP.

Material and Method

Patients, who were diagnosed with OT between March 2010 and January 2011, were identified retrospectively through a database search of three different academic medical centers located in the central Anatolia region in Turkey (Department of Clinical Microbiology and Infectious Diseases, Gulhane Military Medical School, Ankara, Turkey; Fatih University School of Medicine, Ankara, Turkey; and Kirikkale University School of Medicine, Kirikkale, Turkey) after approval from each center's institutional review board. The diagnosis of OT was based on the patient's history and clinical findings compatible with OT, and confirmation was based on the serum micro-agglutination (MA) test. The MA tests were performed at a reference laboratory in central Anatolia (Refik Saydam Hifzıssıhha Laboratory, Ankara, Turkey).

US Protocol: US was performed using a 5–15 MHz linear array transducer (LOGIQ 9, GE Healthcare, Bothell, Washington, USA).

CT Protocol: CT studies were performed using a multislice helical scanner (Aquilion 64, Toshiba Medical Systems, USA). Patients were scanned with 3 mm contiguous axial images from the skull base to the thoracic inlet during intravenous injection of 2 cc/kg of an iodinated contrast agent.

MR Protocol: MR imaging was performed using a 1.5-T superconducting scanner using a standard head neck coil (The New Intera Nova, Philips Medical Systems, Best, The Netherlands) with 30 mT/m gradients. According to the imaging protocol, a T2-weighted turbo spin echo (TSE) sequence and a T1-weighted TSE sequence were obtained in at least two planes using transverse echo-planar diffusion weighted (DW) imaging. ADC maps were calculated using the manufacturer's software. DW sequences were also included in the imaging protocol and ADC values were measured in all lymph nodes.

PET/CT Protocol: Patients were required to fast for 6 hours prior to the study; the blood glucose level was measured and confirmed to be less than 150

mg/dL prior to the study. The patients were asked to rest for 1 hour following the intravenous administration of 370 MBq of 18F-FDG, and the studies were performed at the end of this interval. Imaging was performed on a combined 64-slice PET/CT system (Discovery 690, GE Healthcare, Milwaukee, Wisconsin, USA). Standardized uptake value (SUV) values were measured by a nuclear medicine specialist.

Evaluation of exams: The locations of neck lymph nodes were classified according to the method described by Som et al. [6]. The lymph nodes were evaluated to assess their locations and their morphological characteristics including size, presence of necrosis, presence and type of contrast enhancement, presence of abscess formation, presence of diffusion restriction, and ADC and SUV values. The stage of LAP was also determined through cross-sectional imaging according to the OT classification described by Blanco et al(5). Stage I disease included the presence of firm, enlarged, possibly tender lymph nodes with or without periadenitis, but without signs of necrosis, caseation, or the presence of pus. Stage II disease included the presence of LAP with incipient signs of pus in the lymph nodes or minimal pus (less than 1 cm) in the surrounding tissues. Stage III disease was defined as the presence of a central "necklace sign" indicating an intra-adenopathic abscess or the formation of a necrotic purulent sinus with possible extra-adenopathic extension.

All US, CT, and MRI exams were evaluated by consensus with two radiologists (ATI and CS) and PET/CT exams were evaluated by a radiologist and a nuclear medicine physician (ATI and AA).

Results

A total of 13 patients (10 males, 3 females; mean age 32.62 years; range 12 to 65 years), who were diagnosed with OT by serology (MA titers >1/160), were included in the study. All patients presented to the ENT clinics with complaints of fever, chills, malaise, nausea, sore throat and a painful lump in the neck. Patient 1 also exhibited respiratory distress due to obliterating retropharyngeal LAP. Patient 5 exhibited restricted neck movement due to an invasion and infiltration of the LAP into the right SCM. All patients were unresponsive to conventional antibiotics prior to diagnosis of OT.

The overall results of morphological features for patients with OT are summarized in Table 1. The patients were treated with streptomycin, 7.5-10 mg/kg administered intramuscularly, for fourteen days; doxycycline and/or ciprofloxacin were added if clinically indicated. Gentamicin was the preferred antibiotic in children. All patients underwent blood tests for renal insufficiency before antibiotic therapy was initiated. Two stage III patients, one with a retropharyngeal abscesses and the other with an

abscess that invaded the SCM, required surgical management.

Table 1. Clinical features of patients with oropharyngeal tularemia.

Patient	Age, Gender	Patient's region of origin	Dominant localization (side of neck and lymph node level)	Maximum size of dominant lymph node (cm)	Stage
1	20, M	Çankırı	Right II, VA	1.5x1	I
2	20, M	Çankırı	Bilateral II, III, IV	1x1	II
3	21, M	Çankırı	Bilateral II, III, IV	2x1	I
4	20, M	Kırıkkale	Right II, III	2 x 2	
5	34, M	Kırıkkale	Right II	4 x 3	III
6	63, F	Çankırı	Right IA, retropharyngeal	3x2	III
7	30, F	Kırıkkale	Bilateral II, III, IV	4.5x3	III
8	40, F	Kırıkkale	Bilateral II, left IB	2x1.6	II
9	65, F	Kırıkkale	Bilateral II, III; right IB	2.5x2	I
10	35, M	Çankırı	Bilateral IB, II, III	4x4	III
11	50, F	Yozgat	Right retropharyngeal, left II	3x2	III
12	12, M	Kırıkkale	Left IB	4x2	II
13	14, M	Kırıkkale	Bilateral II, left IB	4.5x3	II

All patients underwent imaging with a combination of techniques including US (n=8), CT (n=5), MRI (n=10), and PET/CT (n=1). US revealed asymmetric LAP with ellipsoid (n=2), round (n=9), or irregular (n=2) shapes. Cutaneous extension and inflammatory stranding of the subcutaneous fat were observed in 1 patient. The lymph nodes involved level I (n=3), level II (n=11), level III (n=6), level IV (n=3), level V (n=1), the parotid space (n=1), and the retropharyngeal space (n=2).

Three patients exhibited large, necrotic lymph nodes, one of which was infiltrating and could not be differentiated from the SCM on sonography. In one patient, sonography revealed strong echoes within the lymph nodes corresponding to calcifications. Loss of the regular nodal shape with spread into the subcutaneous tissue was observed in 2 patients (Figure 1 and 2). On cross sectional evaluation with CT and/or MRI, the lymph nodes were defined as stage I if there were no signs of necrosis, caseation, or pus (n=4). Three patients had stage II disease with incipient signs of pus in the lymph nodes or minimal pus (less than 1 cm) in the surrounding tissues. The remaining 4 patients had stage III LAD with large central necrosis, an abscess or a necrotic purulent sinus with possible extension outside the lymph nodes (Figure 3). The maximum lymph node diameter was approximately 3 cm; one patient had an aggregate of lymph nodes measuring 5x3.5 cm. The most common imaging finding of lymph nodes was heterogeneous enhancement with contiguous low density on CT, high intensity on T2-weighted MR, and ring-enhancement in all patients (Figure 4). Calcification was not observed in any of the CT

studies. The LNs showed diffusion restriction and displayed low ADC values ranging from $0.691 \times 10^{-3} \text{ mm}^2/\text{s}$ to $0.796 \times 10^{-3} \text{ mm}^2/\text{s}$ (Figure 5).

One of the patients underwent a PET/CT scan for the etiologic evaluation of LAP. The mean standard uptake values (SUV) of the lymph nodes were 6.02, which overlapped with malignant LAP (Figure 6). According to our investigation, no other data concerning PET/CT findings in tularemic LAP have yet been published.

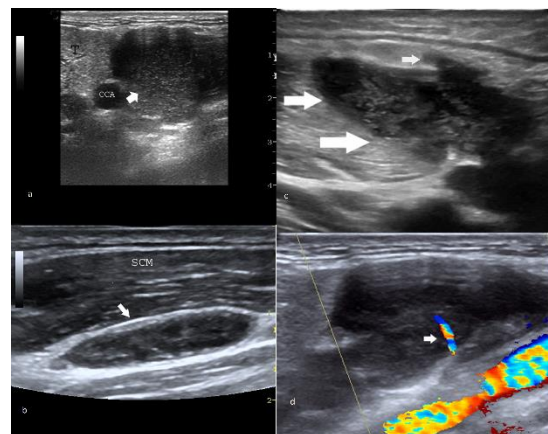


Figure 1. Sonograms through the paramedian neck showing (a) ellipsoid-shaped, (b) round-shaped, and (c) indistinctly shaped lymph nodes (arrows). (d) Doppler ultrasound shows hilar vascularity (arrow) with low resistance flow indicating benign etiology (RI=0.61, PI=0.94).

Discussion

Tularemia occurs endemically in many countries in the northern hemisphere. *Francisella tularensis*

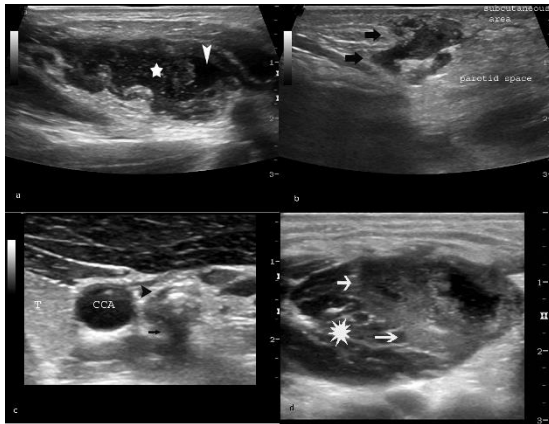


Figure 2. (a) A longitudinal sonogram through a lymph node showing central necrotic debris (star) and necrotic fluid (arrowhead). (b) A sonogram through the right preauricular-parotid area showing subdermal sinus formation (arrows) due to extranodal extension and drainage of the deep lymph nodes. (c) A transverse sonogram through the left paramedian neck showing ring-shaped strong echoes (arrowheads) with posterior shadowing (arrows) that is compatible with calcification in the lymph node. SCM: sternocleidomastoid muscle, T: Thyroid, CCA: Common carotid artery. (d) An axial sonogram showing a necrotic lymph node infiltrating the SCM (arrows). Starburst: SCM.

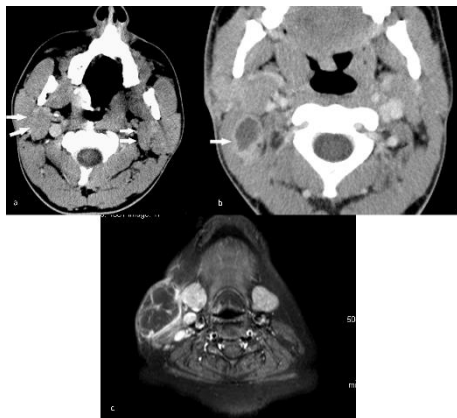


Figure 3. Axial contrast-enhanced CT images showing (a) stage I and (b) stage II LAP (arrows). (c) An axial, fat-suppressed T1 weighted MR image showing stage III LAP.

can infect humans through the skin, mucous membranes, gastrointestinal tract, and the lungs. There is a seasonal grouping of cases in the summer, although tularemia may occur at any time of the year, particularly when climatological conditions facilitate the proliferation of rodents (6). Tularemia principally targets the lymph nodes, lungs and pleura, spleen, liver, and kidney (2). The disease has 6 clinical forms in humans (ulceroglandular, glandular, oculoglandular, oropharyngeal, pneumonic, and typhoidal) depending on the infectious route. OT is contracted by the ingestion of contaminated food or water (2, 7). Symptoms usually begin 3 to 5 days after inoculation and include fever, generalized body aches, headache, chills, and malaise (7). Ulcers may develop in the mouth along with lymph node enlargement. LAP is present in 85% of OT and may be an initial or accompanying sign; sometimes, it is the only presenting sign. Lymph nodes may become fluctuant and may develop into an abscess or drain

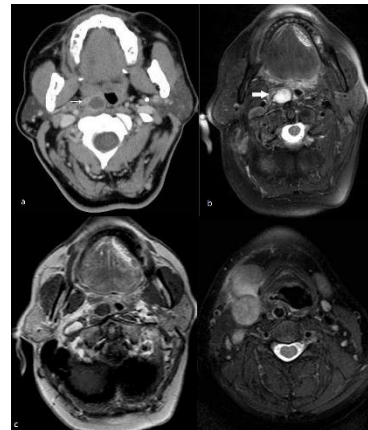


Figure 4. (a) Axial contrast-enhanced CT images showing a hypodense retropharyngeal lesion (arrow). The lesion shows (b) homogenous hyperintensity on the T2-weighted MR image and (c) peripheral enhancement on the post-contrast T1-weighted MR image. (d) The axial, fat-suppressed T2-weighted MR image showing a homogeneous, moderately hyperintense round mass diagnosed as tularemic LAP posterior to the right swollen submandibular gland.

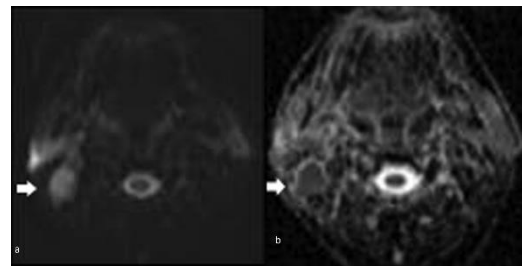


Figure 5. A DW MR image shows an oval mass with restricted diffusion that is (a) hyperintense on a diffusion-weighted image (arrow, b=1000) and (b) hypointense on the ADC map (arrow), suggesting an abscess in a patient with tularemia.

spontaneously. However, they can potentially persist for many months or even years. Due to the difficulty in identifying microorganisms in culture, the diagnosis of OT is mostly based on serological determinations (6).

In the imaging examination of OT, hypertrophy is observed in the tonsils, adenoids and lymph nodes. All lymph node levels can be involved, but LAD is most commonly found in levels II, III and VA. The angles of the mandible and the parotid space are other common sites of involvement. The treatment of OT includes intravenous antibiotics with streptomycin, doxycycline and ciprofloxacin.

Information about the imaging features of tularemic LAP is scarce. Only two papers in the literature have reviewed the CT features of OT. No multimodality imaging tools, including US, MRI and PET/CT, have been performed for the diagnosis of OT in those studies.

US is a widely used non-invasive test for the evaluation of cervical lymphadenopathy. Due to its non-ionizing nature, sonography is an ideal imaging tool for the initial assessment of cervical lymphadenopathy. Homogeneous echotexture can be observed through sonography in the early phase of OT LAP. In the late phase, low central echoes are observed, which suggest necrotic changes. Strong ring-shaped echoes showing calcifications may also

be observed after the treatment of LAP. Both round and ovoid-shaped nodes with distinct margins may be seen on sonography. Abnormal nodal shapes may be observed in patients with extranodal spread of LAP. Extranodal extension may involve the subcutaneous fat, an adjacent salivary gland, or the skin. Doppler ultrasound may reveal hilar vascularity with low resistance flow indicating benign etiology.

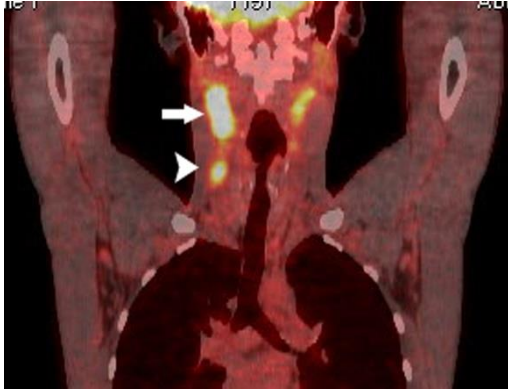


Figure 6. A coronal PET/CT fusion MIP image showing increased FDG uptake in the right level 2 (arrow) and right level III (arrowhead) lymph nodes.

While several molecular mechanisms have been proposed as the basis for FDG uptake in inflammatory lesions, the overexpression of the GLUT-1 subtype in stimulated macrophages, neutrophils, and lymphocytes is considered the most likely cause. In addition, 18F-FDG is not a specific tracer; therefore, it is important to remember that PET/CT scans may be as difficult to interpret in the setting of tularemia as they are with other granulomatous infections or inflammatory conditions such as tuberculosis, sarcoidosis, fungal infections, and malignancy.

Both CT and MRI exhibit certain suggestive imaging features that can adequately define the extent of OT. Both imaging tools show contrast enhancement in LAP, either homogeneously or peripherally. A delay in the initiation of appropriate antibiotic therapy may lead to necrosis, cystic degeneration and abscess formation in lymph nodes. Conglomerated and multiloculated masses with low attenuation centers may exhibit peripheral or septal enhancement consistent with abscess formation (8). Oztoprak et al. reported that when proper antibiotic therapy was delayed 3 weeks, the rate of abscess formation was 20%, the rate of cyst formation was 40% and necrosis occurred in 60% of the lymph nodes; conversely, if the delay was greater than 3 weeks, the rate of abscess formation, cyst formation and the presence of necrosis in the affected lymph nodes was 70%, 100% and 90%, respectively (4).

The differential diagnosis for the imaging appearance of tularemic LAP in the head and neck includes bacterial adenitis, mycobacterial adenitis, cat-scratch disease, fungal infection, brucellosis, infected branchial cleft cyst, infected lymphatic

malformation, treated lymphoma, and other necrotic neoplasms (9-11). Our data suggest that tularemic lymph nodes have a similar imaging spectrum with other infectious diseases, especially with mycobacterial adenitis. Low-density ring-enhancing LAP showing rare cutaneous extension, conglomeration and calcification including in the upper neck levels and the retropharyngeal space are observed in both clinical situations. Clinical findings such as the level of pain associated with LAP can be used to distinguish tularemic LAP from other diseases. For instance, while chronic granulomatous illnesses such as tuberculosis normally exhibit painless LAP, other types of acute adenitis are typically painful.

In this study, we were unable to identify a particular imaging feature that could reliably distinguish tularemic LAP from other forms of LAP. Early diagnosis is essential, because the response to treatment of OT depends mainly on the stage of the infection. The most satisfactory response is observed during the early stages of the infection before suppuration and drainage have occurred. In the early stages, the medical treatment with aminoglycosides (gentamicin, streptomycin), tetracyclines, and fluorinated quinolones is preferred. Surgery is the choice of treatment in some stage II and most stage III patients (6).

This study has several limitations, including the small sample size and the institutional case-selection bias. In addition, it was impossible to determine the time interval between contagion and diagnosis in most of the cases. Thus, we were unable to evaluate the impact of this time interval on our assessment of the imaging findings. Finally, our study did not address the significance of imaging in the diagnosis of different stages of LAP. It is not known whether the imaging findings change with the progressive course of the disease and if so, then at what rate they progress. Serial imaging could potentially address these issues.

In conclusion, OT should be included in the differential diagnosis of unclear cervical LAP that is unresponsive to antibiotic therapy in the endemic areas. Imaging features including low-density ring-enhancing LAP showing rare cutaneous extension, conglomeration and calcification including in the upper neck levels and the retropharyngeal space may suggest the diagnosis of OT.

References

1. Dennis DT, Inglesby TV, Henderson DA, et al. Tularemia as a biological weapon: medical and public health management. *JAMA*. 2001; 285(21):2763–73.
2. Karabay O, Yilmaz F, Gurcan S, Goksugur N. Medical image. Tularaemic cervical lymphadenopathy. *N Z Med J*. 2007 26;120(1248):U2403.
3. Penn RL. Francisella tularensis (tularemia). In: Mandell GL, Bennett JE, Dolin R, editors. *Principles and Practice of Infectious Diseases*, 6th edn. New York: Churchill Livingstone; 2005. p. 2674-85.

4. Oztoprak N, Celebi G, Hekimoglu K, et al. Evaluation of cervical computed tomography findings in oropharyngeal tularaemia. *Scand J Infect Dis.* 2008;40(10):811-4.
5. Coscarón Blanco E, Martín Garrido EP, González Sánchez M, García García I. Clinical study on head and neck tularaemia. *Acta Otorrinolaringol Esp.* 2009;60(1):25-31.
6. Som PM, Curtin HD, Mancuso AA. An imaging based classification for the cervical nodes designed as an adjunct to recent clinically based nodal classifications. *Arch Otolaryngol Head Neck Surg.* 1999;125(4):388-96.
7. Karadenizli A, Gurcan S, Kolayli F, Vahaboglu H. Outbreak of tularaemia in Golcuk, Turkey in 2005: report of 5 cases and an overview of the literature from Turkey. *Scand J Infect Dis.* 2005;37(10):712-6.
8. Jacobs RF. Tularaemia. *Adv Pediatr Infect Dis.* 1997;12:55-69.
9. Robson CD. Imaging of granulomatous lesions of the neck in children. *Radiol Clin North Am.* 2000;38(5):969-77.
10. Kanlikama M, Gokalp A. Management of mycobacterial cervical lymphadenitis. *World J Surg.* 1997;21(5):516-9.
11. Stewart MG, Starke JR, Coker NJ. Nontuberculous mycobacterial infections of the head and neck. *Arch Otolaryngol Head Neck Surg.* 1994;120(8):873-6.